Contents lists available at ScienceDirect

Computers in Biology and Medicine

journal homepage: www.elsevier.com/locate/cbm

Ventricular fibrillation mechanisms and cardiac restitutions: An investigation by simulation study on whole-heart model

Yi Zheng [a], Daming Wei [b,*], Xin Zhu [a], Wenxi Chen [a], Koji Fukuda [b], Hiroaki Shimokawa [b]

[a] Biomedical Information Technology Lab, the University of Aizu, Tsuruga, Ikki-machi, Aizu-Wakamatsu, Fukushima 965-8580, Japan
[b] Department of Cardiovascular Medicine, Tohoku University Graduate School of Medicine, Seiryo-Machi 1-1, Aoba-ku, Sendai, Miyagi 980-8574, Japan

ARTICLE INFO

ABSTRACT

Background: The action potential duration (APD) and the conduction velocity (CV) restitution have been reported to be important in the maintenance and conversion of ventricular fibrillation (VF), whose mechanisms remain poorly understood. Multiple-wavelet and/or mother-rotor have been regarded as the main VF mechanisms, and APD restitution (APDR) and CV restitution (CVR) properties are involved in the mutual conversion or transition between VF and ventricular tachycardia (VT).
Methods and results: The effects of APDR (both its slope and heterogeneity) and CVR on VF organization and conversion were examined using a "rule-based" whole-heart model. The results showed that different organizations of simulated VF were manifestations of different restitution configurations. Multiple-wavelet and mother-rotor VF mechanisms could recur in models with steep and heterogeneous APDR, respectively. Suppressing the excitability either decreased or increased the VF complexity under the steep or shallow APDR, respectively. The multiple-wavelet VF changed into a VT in response to a flattening of the APDR, and the VT degenerated into a mother-rotor VF due to the APDR heterogeneity.
Conclusions: Our results suggest that the mechanisms of VF are tightly related to cardiac restitution properties. From a viewpoint of the "rule-based" whole-heart model, our work supports the hypothesis that the synergy between APDR and CVR contributes to transitions between multiple-wavelet and mother-rotor mechanisms in the VF.

1. Introduction

Sudden cardiac death (SCD) is a major clinical and public health problem in many countries. SCD claims over 300,000 lives annually in the United States alone [1]. Ventricular fibrillation (VF) is notorious as one of the most common causes of SCD [2], but knowledge about VF's underlying mechanisms remains incomplete [3]. It is generally considered that there are two major but contradictory hypotheses on the mechanisms of VF [3–4]: the multiple-wavelet [5] and mother-rotor [6] hypotheses. In addition, the mechanism(s) responsible for the degeneration from reentrant ventricular tachycardia (VT) to VF, conventionally believed to be due to a different mechanism, is not fully understood, either [7].

Weiss et al. [8] in 1999 hypothesized that both the action potential duration (APD) restitution and the conduction velocity (CV) restitution characteristics may be related to the wavelength oscillation that led to wave break, a phenomenon that may convert VT to VF. Clinical studies have either demonstrated [9] or implied [10] that the APD restitution (APDR) is also tightly related to the risk of VF induction. Based on Weiss et al.'s hypothesis, Wu et al. [11] further postulated that both APDR and CV restitution (CVR) were important in VF maintenance, and tested this supposition in experiments using rabbit hearts infused with methoxyverapamil (D600). They found that there were two distinct types of VF during the perfusion of D600 with increasing concentrations: starting from Type 1 VF, then to VT, and finally to Type 2 VF. The Type 1 VF is associated with a steep APDR and a flat CVR, comparable with multiple-wavelet VF. The VT was associated with a flat APDR and a flat CVR. The Type 2 VF was associated with a flat APDR and a steep CVR with a broader CV span, comparable with a mother-rotor VF. Each restitution configuration was associated with a perfusion of D600 at a given concentration. Wu et al. also simulated the transitions from Type 1 VF to VT, to Type 2 VF in a three-dimensional cardiac tissue slab [12].

Since the shape of the real heart is not a slab, the hypothesis tested by simulations in a cardiac tissue slab [12], that the space-time dependent APDR and CVR can significantly influence VF organization and conversion, needs further validation using whole-heart model with a realistic heart shape, because anatomical features can significantly influence wave instability [13]. If both APDR and CVR are indeed important determinants of VF behavior, the manifestations of VF induced in models with some APDR and CVR could reflect these restitution properties. Moreover, the multiple-wavelet VF and the mother-rotor VF and VT would be simulated in models with the corresponding restitution configurations. Furthermore, the transitions from multiple-wavelet VF to VT, to mother-rotor VF from restitution alterations could also be simulated.

Several studies based on whole-heart models investigated the relationship between cardiac restitutions and VF organization. Xie et al. [13] investigated the influence of the APDR slope on VF patterns in a canine ventricular model (by varying the parameter that controls the Ca^{2+} current amplitude, G_{si}), but didn't investigate the effect of the CVR on VF. ten Tusscher et al. [14] tested several factors, including excitability and APDR that determine the number of rotors during VF. Nevertheless, the effects of these factors were only studied individually without investigating the combined action of APDR and CVR in influencing the VF organization. Keldermann et al. [15] have successfully reproduced both multiple-wavelet and mother-rotor VF in a detailed human ventricular model. However, they only investigated the effects of APDR heterogeneity and VF-induction sites on the VF dynamics. To the best of our knowledge, few simulation studies based on a human whole-heart model have been implemented so far to verify the deduction that multiple-wavelet VF, VT, and mother-rotor VF are probably just the different appearances of corresponding APDR and CVR properties, and their mutual conversions are due to changes in restitution. The purpose of this study was to check the role of APDR and CVR in exploring the mechanism of VF [8].

2. Method

We used a "rule-based" model, the Wei–Harumi whole-heart model that contains a detailed description of cellular electrophysiology and cardiac anatomy [16–17] in this study. Its effectiveness is proved by many recognized publications based on this model [18–19]. We enhanced this model's spatial resolution to a finer level 0.5 mm × 0.5 mm × 0.5 mm. Unlike the models reviewed in the previous session, our model included the His–Purkinje system, which is considered to play an important role in the initiation and maintenance of VF

[20–21]. Details and features of this model are provided in the Appendix.

2.1. Electrophysiological settings

We used the APDR and CVR curves in previous publications as an "input" into the Wei–Harumi model. During the simulations, the model cells are assigned time-varying APD and CV according to their APDR, CVR, locations in the model, and the diastolic intervals (DI). The validation of these restitution settings was carefully performed by simulating cardiac processes consistent with clinical reports [22]. The APDR and CVR inputted are described below.

The APDR curves were derived by fitting the clinical discrete data published by Selvaraj et al. [9] to a mono-exponential function [23], as shown below in Eq. (1):

$$APD = APD_{ss} - A \exp(-DI/B) \tag{1}$$

where APD_{ss} is the steady-state APD, A and B are the fitting parameters, and DI is the preceding diastolic interval defined as the amount of time spent recovering prior to an applied stimulus.

Selvaraj et al. defined two data sets recorded from two patients designated as "High-Risk" and "Low-Risk" [9], with each set containing APDR at the apex, middle, and base of the right ventricular (RV) endocardium. Hereinafter, the APDR fitted from the High-Risk and Low-Risk patient data sets will be referred to as "steep" or "shallow" APDR, respectively (see Fig. 1; only the APDR curves at the apex are shown, whose maximum slopes are 1.85 and 0.55, respectively). During the simulation, the effective refractory period (ERP) was part of the APD as introduced in the ERP part of the Appendix, and a ventricular model cell could not be excited by its neighboring model cells if it was in its ERP.

The CVR curves were also depicted using a mono-exponential function similar to Eq. (1). The sources for the CVR were data from the results of ten Tusscher et al. [24] obtained from simulations using a strain of human myocyte model. There were three curves provided in Ref. [24], and two of them were adopted in this study: the standard I_{Na} and the LR I_{Na} CVR curves (obtained from simulations using models with standard and Luo–Rudy (LR) fast I_{Na} dynamics [24], respectively). Both curves were left-shifted by about 56 ms in the abscissa so that the minimum DI value in the later simulations was aligned with the minimum DI value of the steep APDR curve (−33 ms). In addition, the LR I_{Na} restitution curve was scaled up by a factor of 30% to make its steady-state value become 90 cm/s. The transformed LR I_{Na} or standard I_{Na} CVR data (resembling a steep CVR with a broader span or a flat CVR in Ref. [11]) represent physiologically normal excitability or decreased excitability of the cells. Hereinafter, these two CVR will be referred to as "normal" and "decreased" CVR, respectively. During the simulation, the CVR determines the myocyte longitudinal CV dynamically, and the value of CV of an excited cell determined the extent that it could influence (See the "The Propagation Strategy" part in the Appendix). The two solid lines in Fig. 1 show both transformed CVR curves used in the simulation. Note that these two curves are comparable to the CVR acquired from clinical trials [25].

2.2. Models with different restitutions

Table 1 lists the cardiac restitution settings of six different models used in our simulations. It is known that there are different types of electrophysiological heterogeneities in human ventricles, such as the apicobasal gradient, the transmural gradient, and the left–right ventricular heterogeneity [23,25]. These heterogeneities have been proven to play an important role in developing ventricular tachyarrhythmia [15]. The settings of the apicobasal gradient and the transmural gradient have been discussed in the Appendix, and the left–right ventricular heterogeneity was modeled in a simplified manner by assigning different sets of APDR to
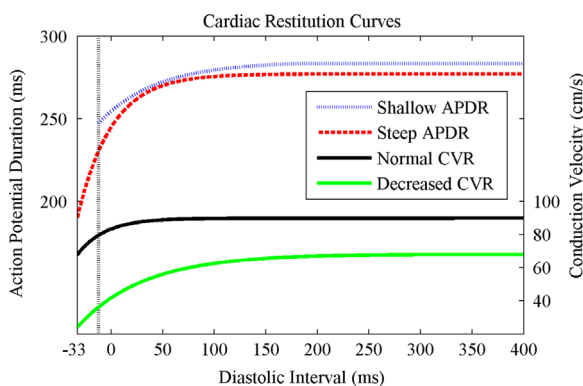
Fig. 1. The action potential duration (APD) and conduction velocity (CV) restitution curves adopted. The dashed lines represent shallow/steep APD restitutions (APDR) at the apex with maximum slope of 0.55/1.85, and the solid lines represent CV restitutions (CVR). The vertical dotted line denotes the minimum diastolic interval (DI) of a shallow APDR.

Table 1
Restitution[a] settings of defined time-invariant models.

Model		Chamber			
		Right ventricle		Left ventricle	
No.	Naming	APDR	CVR	APDR	CVR
1	Steep decreased	Steep	Decreased	Steep	Decreased
2	Steep normal	Steep	Normal	Steep	Normal
3	Shallow decreased	Shallow	Decreased	Shallow	Decreased
4	Shallow normal	Shallow	Normal	Shallow	Normal
5	Hybrid decreased	Shallow	Decreased	Steep	Decreased
6	Hybrid-reverse decreased	Steep	Decreased	Shallow	Decreased

[a] See Fig. 1 for the representative curves of restitution.

the LV and RV (Models 5 and 6 in Table 1, respectively), according to clinical findings that the mean slope of the APDR of the LV can be significantly steeper [25] or shallower [23] than that of the RV. For simplicity, the electrophysiological properties of other cells were unchanged [16], and other pathological heterogeneities (*e.g.* necrosis and fibrosis) were omitted. The VF was induced by successive extra-stimuli applied to the left lateral epicardium.

Furthermore, to model the effect of the admission of D600 in increasing concentrations as reported by Wu et al. [11], Model 2 was duplicated (referred to as the "first stage" in Fig. 5), and its APDR was shallow for a period of ten seconds after removal of any ectopy (referred to as the "second stage" in Fig. 5), and then eight seconds later the CVR was changed to the decreased CVR (modeling a reduced excitability, referred to as the "third stage" in Fig. 5). Hereinafter, this model will be referred to as a "time-variant model", while the other models will be referred to as "time-invariant models".

2.3. Measurements of analysis

The fast Fourier transform (FFT) of a VF episode from the twelfth second to the end of the simulation in the time-invariant models was calculated to assess the overall spectrum. The frequency of interest (FOI) was set to 1–9 Hz (a trade-off of 3–9 Hz in Ref. [26] and 1.5–8 Hz in Ref. [27]), the dominant frequency (DF) was defined as the frequency with the highest peak in the power spectrum [26,28–29], the median frequency (MF) was defined as the frequency that cut the spectrum into two regions with equal total power, and the spectral width (SpW) was defined as the band centered at the MF that covered 67% of the power in the FOI [28]. The upper right-hand image in Fig. 3 shows the locations of the DF, MF (black dotted line), and SpW (the span between the two red lines). These three parameters could describe the metrics of the VF dynamics well [28].

A time–frequency analysis was performed to check the temporal frequency variation during VF in the time-variant model. A short-time FFT was performed with a Gaussian window of 1024 points (3.072 s) shifting stepwise ($\Delta t = 192$ ms) throughout the VF episode [30]. The DF, MF, and SpW values defined above were also determined for each short-time spectrum obtained, and hereinafter are designated as ST-DF, ST-MF, and ST-SpW, respectively. The time–frequency distribution figure was then constructed by plotting the three parameters on the ordinate *vs.* time on the abscissa.

An autocorrelation function for individual VF episodes was generated to evaluate its periodicity, and the *r*-value of the first peak after zero (FPAZ, dimensionless) was used for quantitative comparison [31]. All the objects of our analyses were ECG Lead II traces.

3. Results

3.1. Effects of action potential duration restitution in the time-invariant models

Panel A in Fig. 2 shows the VF organization reproduced using a model with a steep APDR (Model 2). After observing the continuous snapshots of the three-dimension wave-front display, we may intuitively recognize the activation turbulence. The densely scattered dark-blue pixels in the activation map indicate a high incidence of wave breaks where an abrupt dispersion of refractoriness [30] occurred. Furthermore, a chaotic spatiotemporal pattern is highlighted by the random ECG trace in Fig. 2.

In the contrast, the tachyarrhythmia in the model with a shallow APDR (Model 4) showed a significantly higher degree of regularity and periodicity, and is technically regarded as a pleomorphic VT. The snapshots of the wave fronts in Panel B show an example of the VT. The wave fronts originated from the lateral
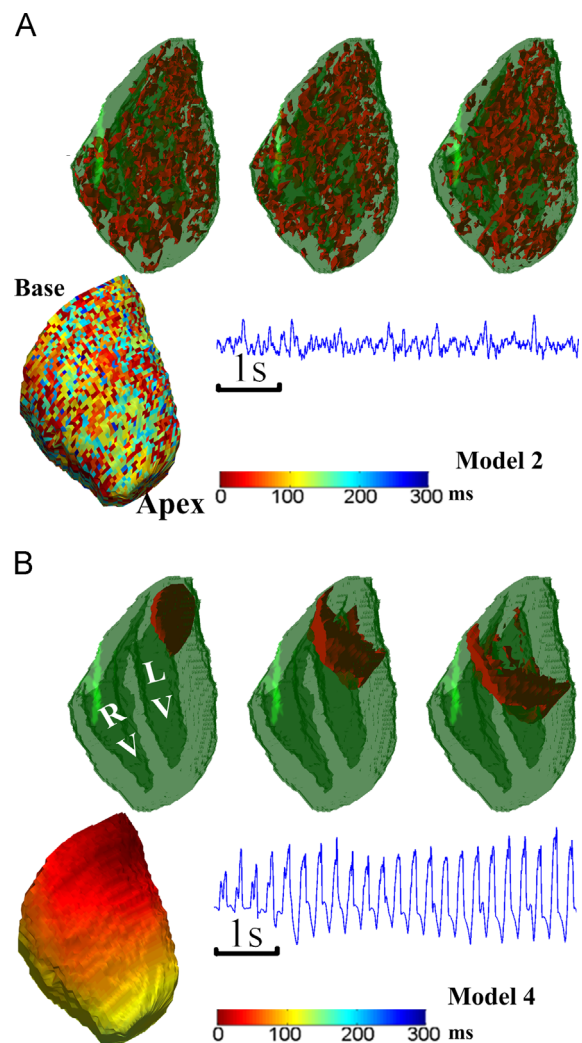
Fig. 2. Illustration of VF dynamics in models with different APDR (atria are not shown). (A) VF induced in a model with a steep APDR (Model 2), and (B) VF induced in a model with a shallow APDR (Model 4). The upper three snapshots are consecutive shots taken 30 ms apart showing the 3-D underlying propagation (wave fronts are shown in red, and the shell of the heart is shown in semi-transparent green). The activation map shows the moment of local excitation time. Both the 3-D wave-front demonstration and the activation map are taken from a left anterior oblique (LAO) view. The ECG trace shows a 6s segment starting from the eighteenth second of the simulation. Key: RV=right ventricle, LV=left ventricle. (For interpretation of the references to color in this figure legend, the reader is referred to the web version of this article.)

endo-LV near the base, and gradually expanded into the vicinity of, and later swept over, the entire cardiac volume. This organized activity might be also manifested by the uniformly distributed activation time. The ECG trace cycle length was stable, around 260 ms, each spike was almost identical, and their amplitude was much larger than that of the ECG in Panel A.

3.2. Effect of conduction velocity restitution in the time-invariant models

Under a steep APDR environment, the VF ECG of models with different CVR were almost the same at first glimpse, but the temporal regularity of the VF in models with decreased CVR (Model 1) was lower than that of the VF in models with normal CVR (Model 2), as evidenced by a comparison between their spectra and the autocorrelations. The spectrum of Model 1 contained multiple frequency peaks over the entire FOI domain, resulting in a broad value of SpW=4.25 Hz, and a notable deviation of the dominant frequency (2.50 Hz) from the median frequency (4.63 Hz). The VF ECG of Model 2 was more organized in the way that the DF value coincided with the MF value (both were 5.38 Hz), and the value of the SpW decreased markedly (2.13 Hz) on comparing it with the value of SpW for Model 1.

However, under a shallow APDR environment, the influence of CVR on VF organization was opposite to that of the steep APDR situation. The VF induced in Model 3 (with decreased excitability) showed a slightly more compact spectrum than the VF in Model 4,

indicating an increased degree of regularity (Fig. 3 Spectrum column, Models 3 and 4).

The autocorrelation plot shown in Fig. 3 summarizes the degree of periodicity of the VF induced in models with different restitution properties, whose FPAZ values were 0.12, 0.42, 0.95, and 0.80 for Models 1, 2, 3 and 4, respectively.

3.3. Effect of heterogeneity in the time-invariant models

There was a relatively stable spiral activation movement in the right ventricular epicardium of Model 5, where the APDR was shallow during VF, as shown in the upper panel of Fig. 4. The spiral wave rotated clockwise around the core (the black asterisk). A single rotation took approximately 240 ms. The wave fronts emitted by this reentrant source managed to propagate coherently through the RV epicardium, but broke up because of intermittent fibrillatory conduction blocks in the LV (as evidenced by the complex distribution of the activation time) where APDR was steep. Its spectrum was characterized by a single peak (4.25 Hz) and a narrow SpW (0.38 Hz).

The VF of Model 6 showed considerable enantiomorphy with the VF discussed above, which is consistent with the restitution distribution. The region where the APDR was shallow also allowed regular propagation, featured by a steady breakthrough (denoted by the black dot in the lower left-hand image of Fig. 4) sending out centrifugal depolarization waves. Its cycle length was about 230 ms. Simultaneously, a continuous formation of wave breaks occurred on the other side of the heart where the APDR was steep. The spectral distribution was more concentrated compared with the VF of Model 5 (SpW=0.13 Hz vs. 0.38 Hz).

Virtual ablations were performed to check whether the VF in Models 5 and 6 was indeed driven by the electrical activity in the shallow APDR regions (RV in Model 5 and LV in Model 6). The removal of mother rotors in the shallow APDR regions did not eliminate the VF. We found that decreasing the mass of ventricles with a steep APDR was a more effective way to eliminate the VF than reducing ventricular tissue with a shallow APDR. For Model 5, the minimum mass with a steep APDR required to sustain VF was approximately 4% of the original ventricular tissue, while the portion for a shallow APDR required to sustain VF was nearly 48%.

## 3.4. Evolution of ventricular fibrillation in the time-variant model

Fig. 5 shows the evolution of VF in the time-variant model. The first stage (denoted by the black line) was the same as the VF induced in Model 2. The VF complexity (i.e., the characteristics of the ECG and activation map) in the time-variant model was reemphasized by its intensive temporal frequency variation. The ST-DF and ST-MF of the first stage fluctuated frequently within a wide band of 2.3–5.9 Hz. The ST-SpW changed widely over a broad range from about 0.98 to 5.9 Hz. This stage matches the description of Type 1 VF [11], or multiple-wavelet VF.

After the APDR flattened (the second stage indicated by the red arrow), the degree of regularity abruptly increased, manifested by the overtly compact spectral distribution, the neat and stable ECG spikes with occasionally varying amplitudes, and the organized activation map, although scattered wave breaks were present. The second stage reproduced the VT well.

Finally, after the excitability was decreased, there was a reduction in organization that cannot be regarded as a return to the initial VF pattern. This reduction was characterized by the temporally varying and changeable frequency content as well as the irregular ECG. It seems that this stage resembles Type 2 VF. Nevertheless, the activation map showed a comparable mode with the second stage, except for the lagged activation time of the distal regions (in green) from the breakthrough (red region) because of the slow conduction velocity.
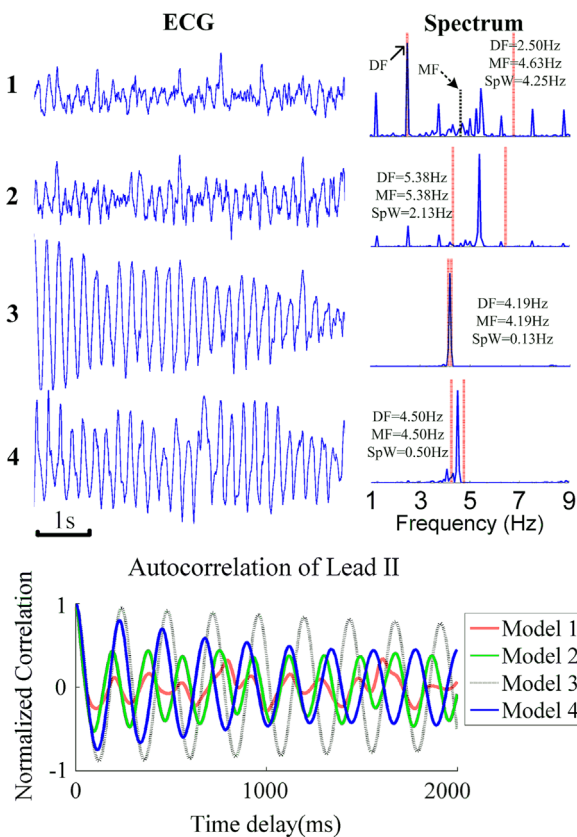
Fig. 3. ECG characteristics of VF induced in the homogeneous models (Models 1 to 4). Upper left-hand side=VF-ECG episodes of 5 s, the digits on the left-hand side denote the model number used. Upper right-hand side=the corresponding ECG spectra. The dominant frequency (DF) denotes the frequency component with the highest amplitude, the median frequency (MF) is denoted by the black dashed line, and the boundaries of the spectral width (SpW) are denoted by the red dotted lines. Lower panel=the autocorrelation of the ECG of the VF induced in the four models. See text for details. (For interpretation of the references to color in this figure legend, the reader is referred to the web version of this article.)
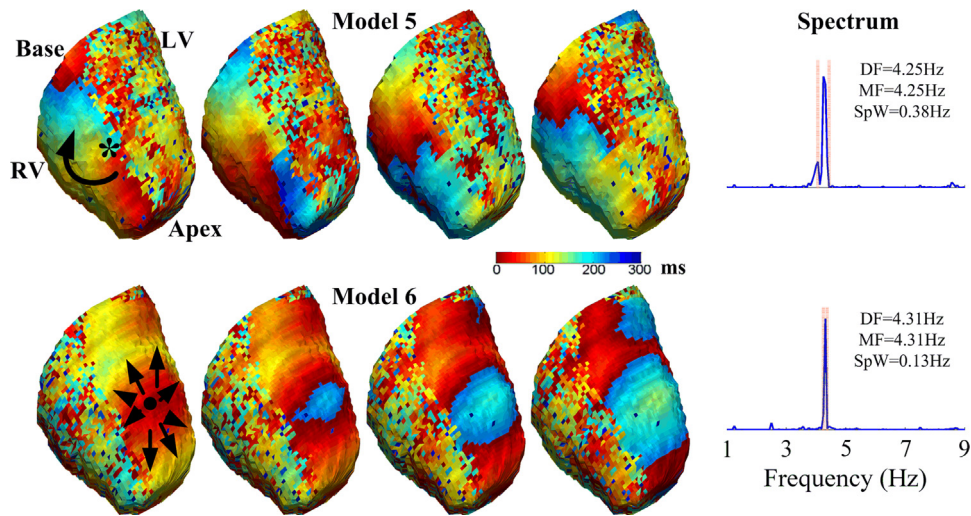
Fig. 4. The behavior of VF induced in the heterogeneous models (Models 5 and 6). The interval between adjacent activation maps was 60 and 30 ms in the upper VF (Model 5) and lower VF (Model 6) groups, respectively. The spiral wave rotated along the direction indicated by the black arrow around the core marked by the black asterisk. The Spectrum column shows the spectra of both VF. The abbreviations used are the same as defined in Fig. 3. Key: RV=right ventricle, LV=left ventricle.
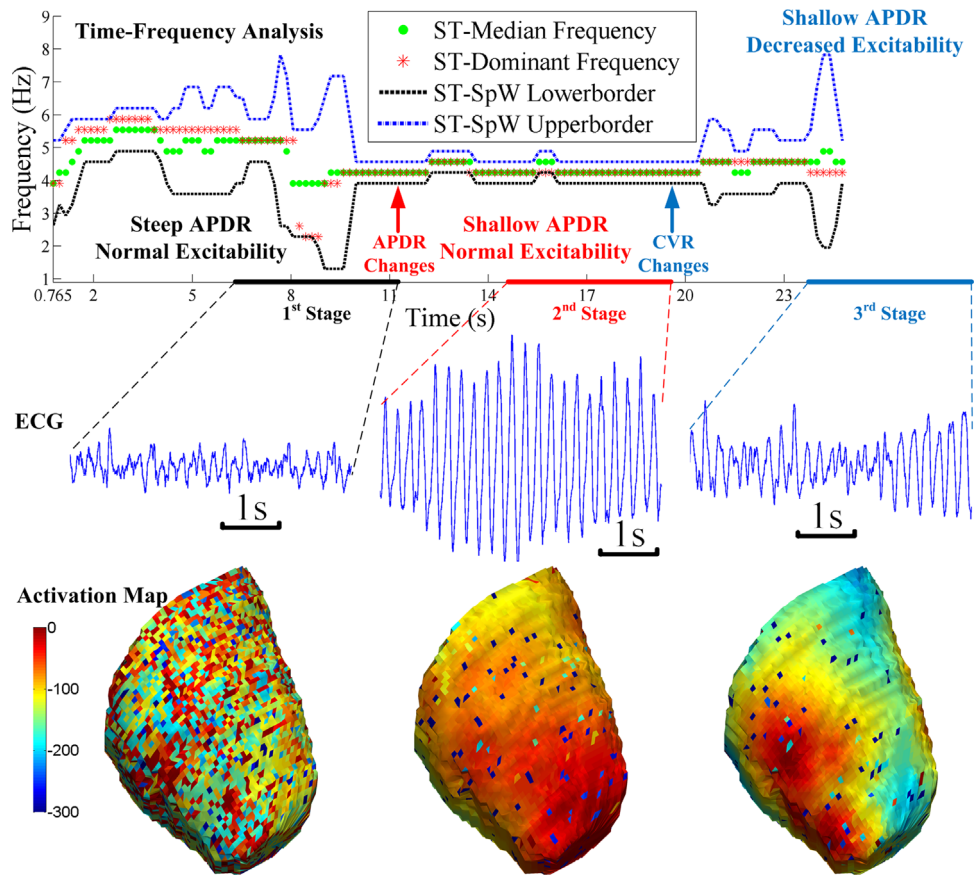

Fig. 5. Simulation of restitution changes. The upper plot shows a time–frequency analysis. The entire trace is divided into three stages separated by the two vertical arrows. The restitution settings of each stage are shown. The middle panel shows the ECG traces of the last 5 s of each stage. The span of each trace is denoted by the bold line orientated along the time axis of the time–frequency analysis. The lower maps are representative activation maps of the three stages. Key: ST=short time.

Thus, the model with restitution properties that varied following the sequence suggested by Wu et al. [11] did not reproduce the transition from VT to Type 2 VF [11] exactly (i.e., the mother-rotor VF).

We found that if the APDR was changed to a heterogeneous process accompanied by a decreased excitability in the third stage, then the VF transition would follow the pattern observed by Wu et al. [11].

Fig. 6 shows the resimulated VF of the third stage after an abrupt transition from VT. There is an obvious decline in regularity on comparison with the VF in the second stage, evidenced by the changeable frequency content in the time–frequency analysis and the ECG. The activation maps were taken at intervals of 60 ms, and depicted VF similar to the VF induced in Model 5, reminiscent of mother-rotor VF.
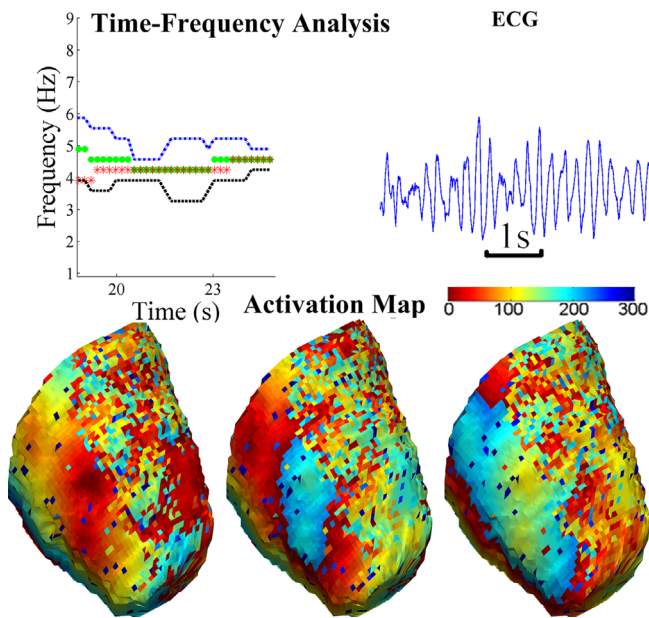
Fig. 6. Situation of a modified "third stage" that reduces the excitability and heterogenizes the APDR. The description of the time–frequency analysis is the same as in Fig. 5. The ECG is the last 5 s episode of the resimulated "third stage". The activation maps are taken at intervals of 60 ms.

4. Discussion

The major new findings of this study are as follows. First, to the best of our knowledge, the present study first simulated the important and well-recognized experimental study by Wu et al. [11] where the conversion from VT to mother-rotor VF was due to the heterogeneity of APD restitution instead of CV restitution flattening. Second, we clarified the effects of the interplay between APD and CV restitution on VF dynamics. Third, the conversion from wavelet VF to VT, and the degeneration from the VT to mother-rotor VF were successfully simulated in a "non-ionic rule-based" whole-heart model.

4.1. Effects of restitution on the VF dynamics

Our simulation data suggest that the slope of the APDR plays a significant role in determining the VF dynamics. In general, a steep APDR corresponds to highly disorganized VF dynamics, and a shallow APDR corresponds to regular VF dynamics.

Idiopathic VF is an uncommon disease of an unknown etiology that occurs in the absence of perceptible organic heart disease or identifiable channelopathy [39], or simply stated, "A healthy heart". It is safe to assume that this type of heart has a shallow APDR and a normal excitability. The tachyarrhythmia induced in the model with this type of restitution (Model 4, Fig. 2B) reproduces the idiopathic VF [40] well. Meanwhile, it is known that structural heart diseases (SHD), such as the old myocardial infarction and hypertrophic cardiomyopathy, may significantly steepen the APDR slope [41]. Simulations show that the VF induced in the models with a steep APDR (Models 1 and 2) also reproduce the multiple-wavelet VF that commonly occurs in patients with SHD, e.g., the DF of the VF induced in Model 2 was 5.38 Hz, slightly exceeding the clinical DF reported by Nash et al. [29] and Masse et al. [27]. Recently, a clinical study by Latcu et al. [42] has shown that the average DF of "fast VF" (DF > 5 Hz) and "slow VF" (DF < 5 Hz) was 5.84 Hz and 4.66 Hz, respectively, which are slightly above the DF values of the VF induced in Model 2 (5.38 Hz) and 4 (4.50 Hz), implying, to a certain extent, that our simulation may explain the VF occurring in these patients. The

different APDR configurations may contribute to the different behaviors between VF correlated with SHD and the idiopathic VF.

The effect of CVR modulating VF dynamics lies with the APDR. When the APDR slope is steep, CVR can markedly influence the VF organization. However, under other APDR settings, the impact of CVR is not so prominent.

The autocorrelation plot in Fig. 3 shows the effect of restitution well. The autocorrelations of the steep APDR are lower than those of the shallow APDR; however, the autocorrelations of a decreased CVR are not always lower than those of a normal CVR, depending on the related APDR. Thus, the synergy between the APDR and CVR determines the VF dynamics, with the APDR taking the leading role.

Apart from the slope of the APDR, the heterogeneity of the APDR may also influence the VF behavior. This confirms the clinical findings of Bueno-Orovio et al. [43]. In the heterogeneous models, the electrical activity was organized in the regions with a shallow APDR and became unstable and broke up in the regions with a steep APDR. The DF values of the VF induced in the heterogeneous models were similar to those of clinical VF obtained during ischemia (3.60 ± 0.04 Hz) [27], which induces heterogeneity because cardiac tissue in different areas has a different tolerance to acute ischemia.

Although it seems that the VF induced in the heterogeneous models (Models 5 and 6) is driven by a breakthrough or spiral wave located in the shallow APDR region, virtual ablation reveals that this could be a false impression. According to the mother-rotor hypothesis, clearing the mother rotor should be a sufficient condition to cease the VF [15], in contrast with our simulations. However, although mother-rotor VF is well observed and documented [44], evidence of terminating VF via ablation is rare, and thus, the causality between the ablation of the mother rotor and VF defibrillation remains to be established [45]. Hence, failing to stop VF with ablation does not necessarily mean that the simulated mother-rotor VF is false, and it is still possible that heterogeneity of the APDR is responsible for the mother-rotor VF. Virtual ablation also suggests that decreasing the amount of tissue with a steep APDR outweighs ablating the shallow APDR regions. Since it is impossible clinically to locate precisely a steep APDR region, admission of a drug that flattens the global slope of the APDR would be a practical way to prevent or convert VF [46].

4.2. Effects of restitution changes and heterogeneity on VF conversion

The restitution changes in the time-variant model followed the sequence reported by Wu et al. [11]. However, only the former two stages reproduced the expected VF well, showing a comparable time course of DF with clinical observation [47]. Although the ECG of the third stage was more irregular than the ECG of the second stage, it did not faithfully reproduce the characteristics of Type 2 VF as predicted by Wu et al. [11]. However, if the restitution changes, that occurred in the third stage, were composed of a decreasing excitability and a heterogenizing APDR, the VT could be converted into Type 2 VF (mother-rotor VF), as shown in Fig. 6. This implies that a decreased CV might only partly contribute to the VF conversion, while the heterogeneity of the APDR may be one of the true causes of the transition from VT to Type 2 VF.

Consequently, our simulation results suggest that Type 1 VF indeed arises from a steep APDR and a normal excitability. The flattening of the APDR slope can convert Type 1 VF into VT, and Type 2 VF is most likely from the heterogeneity of the APDR instead of decreased excitability, or at least the decreased excitability is not the major reason for the conversion from VT to Type 2 VF. Although Wu et al. [11] found that the heterogeneity of the APDR among four recording sites was insignificant after D600 infusion,

the heterogeneity might be masked, because four recording sites may not have fully reflected the overall heterogeneity of the APDR. It is likely that the decreased excitability played an auxiliary role to the heterogeneity and other unknown causes in abruptly converting VT into Type 2 VF. This suggested modification to the deduction of Wu et al. [11] needs further validation. It is worthwhile to note that these factors are in line with the cardiac attributes determining the wave break suggested by Weiss et al. [8].

4.3. The feasibility of the rule-based models

As far as VF is concerned, publications showed that the behaviors of spiral waves and reentry circuits were simulated with both reaction–diffusion models (ionic rule-based models) and cellular automaton models (non-ionic rule-based models) [32–34]. Several studies even could construct a cellular automaton model from "reaction–diffusion" rules to reproduce the simulation of "reaction–diffusion" models [35–38]. So we consider that these two types of heart model should be complementary to each other. On the other hand, in the "rule-based" model, the clinically measured restitutions can be faithfully and quantitatively translated into the simulation rules that govern the cellular dynamics, but it is difficult to do so in the "reaction–diffusion" model. In order to directly examine the relationship between cardiac restitutions and VF dynamics, it is more suitable to use the "rule-based" method for the current study.

4.4. Study limitations

Since the heart model is a finite element model and lacks intercellular current, computational noise may occur. For example, the excitation moment map in Fig. 2A looks noisy at the first glimpse. Nevertheless, we do not think the noise affecting reasonability of the simulation as a whole, because the simulated ECG has comparable waveforms and similar frequency band with the clinical observations, indicating that the simulated cardiac electrical activities well reproduced the behaviors of the VF in vivo, the overall simulation results are still reliable and trustworthy. The APDR and CVR curves were acquired from different studies, so arbitrary combinations of these properties may be unrealistic. Only the heterogeneity of the APDR was considered in our simulations, but a novel technique has revealed considerable heterogeneity in both restitutions [23,25]. It is worth stressing that restitution is not the unique determinant of VF dynamics, and other factors may also play an important role [48]. Some omitted alterations, e.g. the increased gap-junction resistance and fibrotic/necrotic tissues may also affect the VF organizations. The effect of these limitations remains unclear, and shall be investigated in future work.

5. Conclusions

In this study, different types of VF in models with different APDR and CVR setups were simulated using the Wei–Harumi model. Our simulation results suggest that the mechanism of VF has a tight relationship with the cardiac restitution properties. It is likely that the conventional mechanisms of VF can all be explained by the restitution mechanism. In addition, our work supports the hypothesis that the synergy between the APDR (its slope and heterogeneity) and CVR contributes to transitions between multiple-wavelet and mother-rotor mechanisms in the VF. We believe that the results from our simulation study based on a whole-heart model may be significant in understanding the mechanisms of VF, and complement "reaction–diffusion" model-based and experimental studies.

Conflict of interest statement

None declared.

Acknowledgments

Appendix A. Supporting information

Supplementary data associated with this article can be found in the online version at http://dx.doi.org/10.1016/j.compbiomed.2014.06.014.

References

[1] E.D. Engelstein, D.P. Zipes, Sudden cardiac death, in: R.W. Alexander, R.C. Schlant, V. Fuster. (Eds.), The Heart, Arteries and Veins, McGraw-Hill, New York, 1998, pp. 1081–1112.

[2] A.S. Adabag, R.V. Luepker, V.L. Roger, B.J. Gersh, Sudden cardiac death: epidemiology and risk factors, Nature 7 (4) (2010) 216–225.

[3] P.B. Tabereaux, D.J. Dosdall, R.E. Ideker, Mechanisms of VF maintenance: wandering wavelets, mother rotors, or foci, Heart Rhythm 6 (3) (2009) 405–415.

[4] B. Choi, T. Liu, G. Salama, Letter to the editor: ventricular fibrillation: mother rotor or multiple wavelets? Circ. Res. 89 (4) (2001) e30.

[5] G.K. Moe, On the multiple wavelet hypothesis of AF, Arch. Int. Pharmacodyn. Ther. 140 (4) (1962) 183–188.

[6] J. Jalife, Ventricular fibrillation: mechanisms of initiation and maintenance, Annu. Rev. Physiol. 62 (1) (2000) 25–50.

[7] F.H. Samie, J. Jalife, Mechanisms underlying ventricular tachycardia and its transition to ventricular fibrillation in the structurally normal heart, Cardiovasc. Res. 50 (2) (2001) 242–250.

[8] J.N. Weiss, A. Garfinkel, H.S. Karagueuzian, Z. Qu, P. Chen, Chaos and the transition to ventricular fibrillation: a new approach to antiarrhythmic drug evaluation, Circulation 99 (21) (1999) 2819–2826.

[9] R.J. Selvaraj, P. Picton, K. Nanthakumar, V.S. Chauhan, Steeper restitution slopes across right ventricular endocardium in patients with cardiomyopathy at high risk of ventricular arrhythmias, Am. J. Physiol. Heart Circ. Physiol. 292 (3) (2007) H1262–H1268.

[10] P. Taggart, P. Sutton, Z. Chalabi, M.R. Boyett, R. Simon, D. Elliott, J.S. Gill, Effect of adrenergic stimulation on action potential duration restitution in humans, Circulation 107 (2) (2003) 285–289.

[11] T.J. Wu, S.F. Lin, J.N. Weiss, C.T. Ting, P.S. Chen, Two types of ventricular fibrillation in isolated rabbit hearts: importance of excitability and action potential duration restitution, Circulation 106 (14) (2002) 1859–1866.

[12] T.J. Wu, S.F. Lin, A. Baher, Z. Qu, A. Garfinkel, J.N. Weiss, C.T. Ting, P.S. Chen, Mother rotors and the mechanisms of D600-induced type 2 ventricular fibrillation, Circulation 110 (15) (2004) 2110–2118.

[13] F. Xie, Z. Qu, J. Yang, A. Baher, J.N. Weiss, A. Garfinkel, A simulation study of the effects of cardiac anatomy in ventricular fibrillation, J. Clin. Invest. 113 (5) (2004) 686–693.

[14] K.H.W.J. ten Tusscher, R. Hren, A.V. Panfilov, Organization of ventricular fibrillation in the human heart, Circ. Res. 100 (12) (2007) e87–e101.

[15] R.H. Keldermann, K.H.W.J. ten Tusscher, M.P. Nash, C.P. Bradley, R. Hren, P. Taggart, A.V. Panfilov, A computational study of mother rotor VF in the human ventricles, Am. J. Physiol. Heart Circ. Physiol. 296 (2) (2009) H370–H379.

[16] D. Wei, O. Okazaki, K. Harumi, E. Harasawa, H. Hosaka, Comparative simulation of excitation and body surface electrocardiogram with isotropic and anisotropic computer heart models, IEEE Trans. Biomed. Eng. 42 (4) (1995) 343–357.

[17] D. Wei, Whole heart modeling progress principles and applications, Prog. Biophys. Mol. Biol. 67 (1) (1997) 17–66.

[18] E. Ryzhii, D. Wei, Computer simulation of atypical Brugada syndrome, J. Electrocardiol. 42 (4) (2009) 319–327.

[19] X. Zhu, D. Wei, O. Okazaki, Computer simulation of clinical electrophysiological study, Pacing Clin. Electrophysiol. 35 (6) (2012) 718–729.

[20] E.M. Cherry, F.H. Fenton, Contribution of the Purkinje network to wave propagation in the canine ventricle: insights from a combined electrophysiological–anatomical model, Nonlinear Dyn. 66 (1) (2011) 1–15.

[21] L. Li, X. Zheng, D.J. Dosdall, J. Huang, S.M. Pogwizd, R.E. Ideker, Long-duration ventricular fibrillation exhibits 2 distinct organized states, Circ. Arrhythm. Electrophysiol. 6 (6) (2013) 1192–1199.

[22] B.S. Koller, P.E. Karasik, A.J. Solomon, M.R. Franz, Relation between repolarization and refractoriness during programmed electrical stimulation in the human right ventricle: implications for ventricular tachycardia induction, Circulation 91 (9) (1995) 2378–2384.

[23] M.P. Nash, C.P. Bradley, P.M. Sutton, R.H. Clayton, P. Kallis, M.P. Hayward, D.J. Paterson, P. Taggart, Whole heart action potential duration restitution properties in cardiac patients: a combined clinical and modelling study, Exp. Physiol. 91 (2) (2006) 339–354.

[24] K.H.W.J. ten Tusscher, A.V. Panfilov, Alternans and spiral breakup in a human ventricular tissue model, Am. J. Physiol. Heart Circ. Physiol. 291 (3) (2006) H1088–H1100.

[25] A.M. Yue, M.R. Franz, P.R. Roberts, J.M. Morgan, Global endocardial electrical restitution in human right and left ventricles determined by noncontact mapping, J. Am. Coll. Cardiol. 46 (6) (2005) 1067–1075.

[26] S. Masse, E. Downar, V. Chauhan, E. Sevaptsidis, K. Nanthakumar, Ventricular fibrillation in myopathic human hearts: mechanistic insights from in vivo global endocardial and epicardial mapping, Am. J. Physiol. Heart Circ. Physiol. 292 (6) (2007) H2589–H2597.

[27] S. Masse, T. Farid, P. Dorian, K. Umapathy, K. Nair, J. Asta, H. Ross, V. Rao, E. Sevaptsidis, K. Nanthakumar, Effect of global ischemia and reperfusion during ventricular fibrillation in myopathic human hearts, Am. J. Physiol. Heart Circ. Physiol. 297 (6) (2009) H1984–H1991.

[28] J.F. Huizar, M.D. Warren, A.G. Shvedko, J. Kalifa, J. Moreno, S. Mironov, J. Jalife, A.V. Zaitsev, Three distinct phases of VF during global ischemia in the isolated blood-perfused pig heart, AJP – Heart Circ. Physiol. 293 (3) (2007) H1617–H1628.

[29] M.P. Nash, A. Mourad, R.H. Clayton, P.M. Sutton, C.P. Bradley, M. Hayward, D.J. Paterson, P. Taggart, Evidence for multiple mechanisms in human ventricular fibrillation, Circulation 114 (6) (2006) 536–542.

[30] G. Salama, B.R. Choi, Imaging ventricular fibrillation, J. Electrocardiol. 40 (6 Suppl.) (2007) S56–S61.

[31] N.A. Lever, E.G. Newall, P.D. Larsen, Differences in the characteristics of induced and spontaneous episodes of ventricular fibrillation, Europace 9 (11) (2007) 1054–1058.

[32] C.W. Zemlin, A.V. Panfilov, Spiral waves in excitable media with negative restitution, Phys. Rev. E: Stat. Nonlinear Soft Matter Phys. 63 (4.1) (2001) 41912.

[33] G. Bub, A. Shrier, L. Glass, Spiral wave generation in heterogeneous excitable media, Phys. Rev. Lett. 88 (5) (2002) 58101.

[34] F. Alonso Atienza, J. Requena Carrion, A. Garcia Alberola, J.L. Rojo Alvarez, J.J. Sanchez Munoz, J. Martinez Sanchez, M. Valdes Chavarri, A probabilistic model of cardiac electrical activity based on a cellular automata system, Rev. Esp. Cardiol. 58 (01) (2005) 41–47.

[35] O. Bandman, Simulating spatial dynamics by probabilistic cellular automata, Lect. Notes Comput. Sci. 2493 (2002) 10–19.

[36] O. Bandman, Accuracy and stability of spatial dynamics simulation by cellular automata evolution, Lect. Notes Comput. Sci. 2763 (2003) 20–34.

[37] O. Bandman, Computation properties of spatial dynamics simulation by probabilistic cellular automata, Future Gener. Comput. Syt. 21 (5) (2005) 633–643.

[38] A. Nishiyama, Construction of an isotropic cellular automaton for a reaction – diffusion equation by means of a random walk, J. Phys. Soc. Jpn. 80 (2011) 54003.

[39] S. Viskin, B. Belhassen, Idiopathic ventricular fibrillation, in: I. Gussak, C. Antzelevitch, A.A.M. Wilde, P.A. Friedman, M.J. Ackerman, W. Shen. (Eds.), Electrical Diseases of the Heart - Genetics, Mechanisms, Treatment, Prevention, Springer, London, UK, 2008, pp. 588–603.

[40] H. Kasanuki, S. Ohnishi, M. Ohtuka, N. Matsuda, T. Nirei, R. Isogai, M. Shoda, Y. Toyoshima, S. Hosoda, Idiopathic ventricular fibrillation induced with vagal activity in patients without obvious heart disease, Circulation 95 (9) (1997) 2277–2285.

[41] M.L. Koller, S.K.G. Maier, A.R. Gelzer, W.R. Bauer, M. Meesmann, R.F.J. Gilmour, Altered dynamics of action potential restitution and alternans in humans with structural heart disease, Circulation 112 (11) (2005) 1542–1548.

[42] G.D. Latcu, O. Meste, A. Duparc, P. Mondoly, A. Rollin, M. Delay, P. Maury, Temporal and spectral analysis of ventricular fibrillation in humans, J. Interv. Card. Electrophysiol. 30 (3) (2011) 199–209.

[43] A. Bueno-Orovio, B.M. Hanson, J.S. Gill, P. Taggart, B. Rodriguez, in vivo human left-to-right ventricular differences in rate adaptation transiently increase pro-arrhythmic risk following rate acceleration, PLoS ONE 7 (12) (2012) e52234.

[44] M. Vaquero, D. Calvo, J. Jalife, Cardiac fibrillation: from ion channels to rotors in the human heart, Heart Rhythm 5 (6) (2008) 872–879.

[45] P.S. Spector, D.D. Correa De Sa, E.S. Tischler, N.C. Thompson, N. Habel, J. Stinnett-Donnelly, B.E. Benson, P. Bielau, J.H.T. Bates, Ablation of multi-wavelet re-entry: general principles and in silico analyses, Europace 14 (Suppl. 5) (2012) v106–v111.

[46] S. Ashino, I. Watanabe, M. Kofune, K. Nagashima, K. Ohkubo, Y. Okumura, H. Mano, T. Nakai, S. Kunimoto, Y. Kasamaki, A. Hirayama, Effects of quinidine on the action potential duration restitution property in the right ventricular outflow tract in patients with brugada syndrome, Circ. J. 75 (9) (2011) 2080–2086.

[47] C.P. Bradley, R.H. Clayton, M.P. Nash, A. Mourad, M. Hayward, D.J. Paterson, P. Taggart, Human ventricular fibrillation during global ischemia and reperfusion, Circ. Arrhythm. Electrophysiol. 4 (5) (2011) 684–691.

[48] B.O. Bingen, S.F.A. Askar, M.J. Schalij, I.V. Kazbanov, D.L. Ypey, A.V. Panfilov, D.A. Pijnappels, Prolongation of minimal action potential duration in sustained fibrillation decreases complexity by transient destabilization, Cardiovasc. Res. 97 (1) (2013) 161–170.